

pubs.acs.org/acsapm Article

Enhancing Toughness of Post-Consumer Recycled Polyolefins with Polybutadiene-Derived Block Copolymers

Gabriela Díaz Gorbea, Liyang Shen, Kendra Flanigan, Christopher J. Ellison,* and Frank S. Bates*



Cite This: ACS Appl. Polym. Mater. 2024, 6, 12691-12699



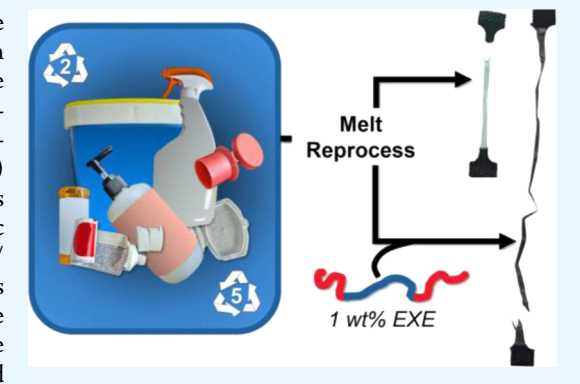
ACCESS I

III Metrics & More

Article Recommendations

Supporting Information

ABSTRACT: There is a rapidly expanding need for economically viable approaches for ameliorating the wasteful disposal of post-consumer plastics in landfills and the leakage of these materials into the environment. Here, we assess the efficacy of poly(ethylene)-block-poly(ethylene-ran-ethyl ethylene)-block-poly(ethylene) (EXE) triblock copolymers as compatibilizers in post-consumer recycled poly(ethylene) (rPE) and isotactic polypropylene (rPP) containing ca. 10–15% PP and PE impurities, respectively. $E_{67}X_{138}E_{67}$ was prepared by anionic polymerization of butadiene followed by catalytic hydrogenation, where the subscripts indicate block molecular weight in kg/mol. This triblock copolymer was mixed with rPE and rPP, along with blends formed from virgin PE and PP, and the recycled and blended materials were characterized by differential scanning calorimetry (DSC), atomic force microscopy (AFM), and tensile testing. The presence of phase-separated



impurities in the recycled plastics was confirmed by DSC and AFM, and shown to contribute to inferior mechanical properties, e.g., strain at break, $\varepsilon_{\rm b} < 20\%$ for melt-molded specimens cooled at 38 °C/min, referred to as fast cooling. Addition of 1 wt % of $\rm E_{67}X_{138}E_{67}$ to rPE and rPP led to improvements in ductility, dependent on the rate of cooling of melt-molded specimens. Fast cooling produced marginal gains in ductility, $\varepsilon_{\rm b} \approx 90$ and 30% in rPE and rPP, respectively. However, industrially relevant very fast cooling (380 °C/min) dramatically improved the ductility, where $\varepsilon_{\rm b} \geq 500\%$ for both recycled plastics. Similar results were obtained with virgin PE/PP blends containing 1 wt % $\rm E_{67}X_{138}E_{67}$. These findings are compared with the results described in a previous report, where 1 wt % $\rm E_{65}X_{88}E_{65}$ was added to virgin PE/PP blends, indicating that the X block molecular weight plays an important role in the efficacy of compatibilization.

KEYWORDS: anionic polymerization, copolymer, AFM, ductility, recycled plastics

1. INTRODUCTION

Plastics are an essential part of modern life, combining durability, versatility, and low cost, but they typically persist for tens to hundreds of years after entering the waste stream and environment. In the packaging sector, it is estimated that greenhouse gas emissions are 69% lower by using plastic rather than alternatives such as paper, aluminum, and glass.¹ Unfortunately, global plastic waste generation rates are increasing while the percentage of produced plastics that are recycled is decreasing.²-5 Polyethylene (PE) and isotactic polypropylene (PP) together account for over 60% of plastic waste generation making them important targets for sustainability efforts.^{6,7}

Recycling is considered an essential element for addressing this global crisis. Mechanical recycling is currently the most established route where mixed plastic waste is collected in materials recovery facilities (MRFs), sorted into constituents, chopped, washed, and melt-reprocessed into recycled resins. However, the output quality remains low due to difficulties in sorting mixtures, which currently rely on near-IR spectroscopy (NIR) and water flotation as the main separation techniques.

PE and PP have similar mass densities and NIR spectral signatures, making sorting challenging, especially with material flow rates of thousands of kg/h.^{2,10} As a result, the flake sold as post-consumer recycled (PCR) PE or PP often possesses purities ranging from 70 to 90%. Melt-reprocessing of impure recyclates results in heterogeneous, macrophase-separated blend materials with poor mechanical properties. Compatibilizer additives can improve the properties of PE and PP blends, and there is a great need for potent and economical versions that could be produced by existing commercial processes.

Block copolymers are commonly used as compatibilizers, either by incorporating precursors that react *in situ* at interfaces¹¹ or by adding premade block copolymers during melt-compounding. Effective compatibilizers localize at

Received: July 21, 2024
Revised: October 7, 2024
Accepted: October 8, 2024
Published: October 16, 2024





Scheme 1. EXE Triblock Copolymer Structure (x = 0.06 and y = 0.86)

blend component interfaces reducing interfacial tension and dispersed phase domain sizes while also improving interfacial adhesion. Premade block copolymers are the most common for polyolefin compatibilization, although a few studies have explored reactive systems that usually require other additives to promote reactions, such as catalysts or oxidants. Remarkable progress has been made in premade compatibilizer synthesis, characterization, and implementation of both graft and linear copolymer architectures. Notably, multiblock copolymers with alternating PE and PP blocks have been demonstrated to effectively compatibilize PE/PP blends at only 0.2 wt % loading. However, the required amount of the hafnium-based catalysts used in the synthesis and expected cost make this approach impractical.

We recently demonstrated the efficacy of poly(ethylene)block-poly(ethyl ethylene-ran-ethylene)-block-poly(ethylene) (EXE) triblock copolymer compatibilizers in virgin PE/PP blends, in analogy to mechanical recycling of a common mixed waste stream.²⁵ The synthesis of EXE exploits facile anionic polymerization of 1,3-butadiene and catalytic hydrogenation, materials and processes used today in commercial polymer production. EXE compatibilizers possess semicrystalline E end blocks that are miscible with PE and an amorphous X midblock that is melt miscible with PP due to conformational asymmetry effects²⁶ facilitating localization at PE/PP interfaces. PE/PP blends with EXE loadings of 1 wt % exhibited improved strain at break (ε_b) of ~500% compared to \leq 40% for neat blends, which was supported by microscopic evidence revealing significant interfacial adhesion between PE and PP domains. We proposed an interfacial adhesion mechanism termed "threading the needle" involving anchoring of EXE by topological entanglement of the PP-miscible amorphous X block²⁷ loops (i.e., eye of the needle) with PP homopolymer (i.e., the thread) while the E end blocks anchor into the adjoining PE domain by cocrystallization of the E block with PE homopolymer.²⁵ In this paper, we evaluate the compatibilization efficacy of another EXE triblock copolymer with a different X block molecular weight at a similar E block molecular weight. Additionally, we focus on evaluating the performance of EXE in post-consumer recycled PE (rPE) and PP (rPP), blends that represent more practically relevant waste streams than virgin PE/PP blends.

2. EXPERIMENTAL SECTION

2.1. Materials. Virgin high-density polyethylene (HDPE) (DMDA 8904, MFI 4.4 g/10 min at 190 °C with 2.16 kg) and isotactic PP (H314–02z, MFI 2.0 g/10 min at 230 °C with 2.16 kg) used in this work were sourced from Dow Chemical Company. The recyclates used, rPE (KWR 105–7525, MFI 2.0 g/10 min at 190 °C with 2.16 kg) and rPP (KWR 621, MFI 10 g/10 min at 230 °C with 2.16 kg), were generously provided by KW Plastics.

Mixed microstructure polybutadiene triblock copolymer was synthesized through sequential anionic polymerization of 1,3-butadiene, containing 94% 1,4-addition for the first block and 86% 1,2-addition for the second block followed by coupling of the living diblocks through addition of dichlorodimethylsilane coupling agent at

half the molar concentration of anions. Further details of the 1,4-PB-block-1,2-PB-block-1,4-PB synthesis can be found in our previous work. The resultant triblock copolymer was then hydrogenated using a homogeneous catalyst. For 5 g of polymer charged to the hydrogenation reactor, 180 mg of chloridotris(triphenylphosphine)-rhodium(I) (Wilkinson's catalyst) was used along with 1 g of triphenylphosphine in 0.5 L of toluene. The reactor was pressurized to 500 psig of hydrogen and allowed to react for 12 h at 100 °C. Following saturation, the polymer underwent at least three cycles of dissolution in hot toluene followed by precipitation in methanol to remove any remaining catalyst. EXE was then dried under vacuum at 40 °C for 72 h. Scheme 1 depicts the final product where x = 0.06 and y = 0.86.

2.2. Molecular Characterization Methods. Molecular weight determination of both virgin and recycled PE and PP was carried out using an Agilent PL-GPC 220 high-temperature size exclusion chromatography (SEC) system equipped with a differential refractive index detector, and a Wyatt DAWN HELEOS II multiangle light scattering detector. Samples were run using 1-2 mg/mL concentrations of polymer in 1,2,4-trichlorobenzene (TCB) eluent at 150 °C, with an injection volume of 100 μ L and a flow rate of 1 mL/min. Normalized refractive index traces are shown for PE, PP, rPE, and rPP in Figure S1. Light scattering measurements, based on differential refractive index increment, dn/dc, values were used for absolute molecular weight determination of PE (-0.110 mL/g at 150 °C)³⁰ and PP $(-0.103 \text{ mL/g} \text{ at } 150 \,^{\circ}\text{C})^{31}$ samples. The molecular weight of E₆₇X₁₃₈E₆₇ was characterized with an Agilent PL-GPC using the same sample concentration at 135 °C and dn/dc = -0.103 mL/g.³⁰ Peak deconvolution analysis of the $E_{67}X_{138}E_{67}$ block copolymer was performed and revealed a coupling efficiency of $\sim\!80\%$, as shown in Figure S2 and Table S1. 25

The molecular weight for the unsaturated PB precursor samples was determined using a Viscotek GPC max VE 2001 equipped with three Agilent PL Gel Mixed-C columns and a Viscotek 270 dual detector and operated at 25 °C. Sample concentrations ranged from 1 to 2 mg/mL in inhibited ACS-grade tetrahydrofuran (THF) and an injection volume of 100 μ L. Molecular weight determination used universal calibration with polystyrene standards with Mark–Houwink–Sakaruda constants $a_{\rm PS}=0.736$ and $K_{\rm PS}=0.863\times10^{-4}$ dL/g for polystyrene, 32 $a_{\rm 1,4-PB}=0.670$ and $K_{\rm 1,4-PB}=4.57\times10^{-4}$ dL/g for 1,4-PB with 6% vinyl fraction, and $a_{\rm 1,2-PB}=0.670$ and $K_{\rm 1,2-PB}=3.90\times10^{-4}$ dL/g for 1,2-PB with 86% vinyl fraction. 33 The constants for 1,4-PB and 1,2-PB were acquired through linear extrapolation of K values for PB samples with varying vinyl fractions ranging from 8 to 73%. 33

Block copolymer microstructural compositions of the PB precursors were evaluated through room-temperature ¹H NMR using a Bruker AX 400 with a 30 s relaxation delay and sample concentrations of 10–20 mg/mL in chloroform-d. The EXE block copolymer was characterized at 90 °C using a Bruker AV 500 with a 10 s relaxation delay and sample concentrations of 10–20 mg/mL in toluene-d8. Figures S3 and S4 show the NMR spectra for each sample as well as the coupled and hydrogenated final samples with the associated integrations in Table S2. Tables S2 and S3 summarize the properties of both EXE block copolymers investigated in this work.

2.3. Thermal Characterization. A Mettler Toledo DSC1 differential scanning calorimeter (DSC) operated with a nitrogen purge gas flow rate of 50 mL/min and employing 40 μ L flat aluminum pans was used to characterize the polymer thermal properties. Calorimetric data were taken following a first heating to remove thermal processing history, unless noted otherwise. Data are reported

normalized by sample weight (ca. 5-10 mg). Melting temperature was obtained from the peak values in the second heating scan at a rate of 10 °C/min up to 200 °C. Glass transition temperatures, $T_{\rm g}$, are reported as the midpoint value upon heating from −100 °C at a heating rate of 10 °C/min during the second heating cycle. The DSC traces for $E_{65}X_{88}E_{65}$ and $E_{67}X_{138}E_{67}$ are given in Figure S5. The effects on crystallinity upon adding E₆₇X₁₃₈E₆₇ to either rPE or rPP were evaluated using cooling and second heating DSC traces, as shown in Figure S6 and summarized in Table S4. Crystallinity was determined using a weighted average of the enthalpies of fusion at 100% crystallinity of PE ($\Delta H_{\text{PE},100\%} = 289 \text{ J/g}$)^{34,35} and PP ($\Delta H_{\text{PP},100\%} =$ 170 J/g).³⁶ The purity of rPE and rPP was determined to be approximately 85 and 90%, respectively, via a combination of DSC and AFM measurements (Table S5).

2.4. Rheological Properties. Rheological data were collected for virgin PE, virgin PP, rPE, and rPP using a TA Instruments ARES-G2 rheometer operated under a nitrogen purge with an 8 mm parallel plate geometry and an ~0.5 mm gap. Frequency sweeps spanning 0.1 to 100 rad/s were conducted at temperatures ranging from 170 to 200 °C within the linear viscoelastic regime, at strain amplitudes of 5 to 10%. Rheological characterization and analyses for commercial virgin PE and PP and rPE and rPP are given in Figures S7 and S8, respectively, and summarized in Table S6.

2.5. Blend Preparation and Tensile Testing. Blends were prepared using a recirculating twin screw microcompounder (XPlore 15 cm³) set to 190 °C, under a N₂ purge, and operated at 130 rpm for 12 min. To study the effect of $E_{67}X_{138}E_{67}$ on PE/PP blends (or rPE and rPP) in comparison to $E_{65}X_{88}E_{65},$ compatibilizers were added at either a 1 or 1.7 wt % total loading concurrently with PE and PP pellets in a 70:30 or 30:70 (PE/PP) weight-based composition. Extruded material was molded in a Wabash platen press into 0.5-mmthick films by first annealing for 5 min at 180 °C, pressing at 3000 lb for 5 min at the same temperature, followed by cooling using one of the two procedures depicted in Figure S9. Representative temperature profiles were acquired using a k-type thermocouple embedded in a film sample for both cooling procedures, as illustrated in Figure S10. Fast cooling (~38 °C/min), used in all comparisons between $E_{65}X_{88}E_{65}$ and $E_{67}X_{138}E_{67}$, employed cooling water in a press that was turned on at the end of the pressing cycle without releasing pressure. Very fast cooling (~380 °C/min) was achieved by transferring the film samples (held in a metal frame) from the hot press to a watercooled second press held at 10 °C. Dumbbell-shaped tensile bars were die-cut (ASTM D1708, 5 mm gauge width, 22 mm gauge length) and tested at room temperature using an Instron 5966 Universal Testing System operated at a crosshead speed of 22 mm/min (100%/min strain rate).²⁵ Tensile data are given in Figures S11 and S12 for the virgin blends and in Figures S13 and S14 for the rPE and rPP samples. Properties are summarized in Tables S7 and S8 for the virgin blends and in Table 3 for the recycled samples.

2.6. Imaging Techniques. Tensile specimens of compatibilized and uncompatibilized rPE and rPP were cryofractured in liquid nitrogen and examined using a Hitachi SU8230 field emission scanning electron microscope (SEM) operated with a 5 kV accelerating voltage and approximately 10 mm working distance. Specimens were affixed with carbon tape to a 90° pin stub mount and sputter coated with a 5-nm-thick platinum conducting layer to minimize charging effects. SEM images are provided in Figure S15.

Phase morphology was characterized by AFM using a Bruker Nanoscope V Multimode 8, Digital Instruments open-loop atomic force microscope system operated in dynamic mode. Smooth imaging surfaces were obtained from pressed and annealed films using a Leica UC6 cryo-ultramicrotome at −120 °C. To create a cutting face, a DiaTOME CT369 Cryotrim45 diamond knife with a 6° clearance angle was used, followed by sectioning of 500-nm-thick slices using a DiaTOME size 4 H12841 Hystocryo45 diamond knife. Slices were mounted on a silicon wafer and imaged in the repulsive regime by using an n-type silicon tip cantilever (resonant frequency = 166 Hz, spring constant = 2 N/m, and radius = 8 nm).

AFM images were processed using Gwyddion 2.56 open-source software to level the data, align rows, correct scarring, and adjust the contrast. Particle measurements were carried out using ImageI software to acquire the droplet dimensions. Extracted diameters were multiplied by a factor of $4/\pi$ to correct for the fact that microtoming does not section through the center of each particle.³ Size distributions were fit to log-normal curves to extract average particle diameters and standard deviations. Phase images comparing the morphologies of fast-cooled and very fast-cooled recyclates are given in Figure S16. Histograms and AFM images for the measurements are given in Figures S17-S19 and summarized in Table S9.

3. RESULTS AND ANALYSIS

3.1. Characterization of EXE. Characterization data for the two EXE block copolymers referred to in this study are summarized in Table 1.

Table 1. Characterization of EXE Samples

	$M_n \pmod{kDa}$	f_{X} $(\%)^{c}$	Đ	$(^{\circ}C)^{d}$	$({}^{\circ}C)^{e}$	$({}^{\circ}C)^{f}$
E ₆₅ X ₈₈ E ₆₅	176ª	40	1.2 ^a	104	87	-28
$E_{67}X_{138}E_{67}$	204 ^b	47	1.1^{b}	112	88	-33

^aFrom ref 25 based on universal calibration of SEC results. ^bDetermined by SEC using light scattering detection. ^cVolume fraction of X block, determined by 1H NMR and using polymer densities. ^dMelting temperature of E blocks determined by DSC while heating at 10 °C/min. eCrystallization temperature of E blocks determined by DSC while cooling at 10 °C/min. fGlass transition temperature of X block determined by DSC while heating at 10 °C/ min.

SEC traces for each stage of the PB synthesis are shown in Figure 1a. The microstructure of the X block in $E_{67}X_{138}E_{67}$ was determined to be y = 0.86 (Scheme 1) based on ¹H NMR measurement of the 1,4-PB-block-1,2-PB diblock sampled from the reactor prior to coupling into the triblock architecture; separate ¹H NMR characterization of 1,4-PB homopolymer first block produced the well-established result x = 0.06 (see Figures S3 and S4).²⁷ SEC traces were also used to determine a diblock coupling efficiency of approximately 80% (see Figure S2), comparable to what was previously reported for E₆₅X₈₈E₆₅. Hydrogenation of the polybutadiene triblock produced >99% saturation and no significant change in total molecular weight while retaining a narrow, monomodal molecular weight distribution, as shown in the SEC trace in Figure 1b.

3.2. Characterization of Majority Blend Components. The rPE and rPP pellets used in this study were both opaque and black or gray, respectively, presumably due to the presence of impurities such as dyes and possibly carbon black. The molecular weight and thermal characterization for both the virgin and recycled resins used in this study are summarized in Table 2. Figure 2 shows DSC traces for rPE and rPP, which both contain two distinct endothermic peaks upon heating, corresponding to the melting temperatures of PE and PP. Additionally, the cooling data show two crystallization peaks, again consistent with the presence PE contaminant in rPP and PP contaminant in rPE. The contamination most likely arises from the difficulty in cleanly sorting the two polyolefins, which have similar mass densities, making flotation difficult, and similar infrared spectra, making spectroscopic identification challenging. The percentages of polyolefin impurities in each recycled material were estimated using the DSC heating data (Figure 2) and area analysis of AFM images, as summarized in

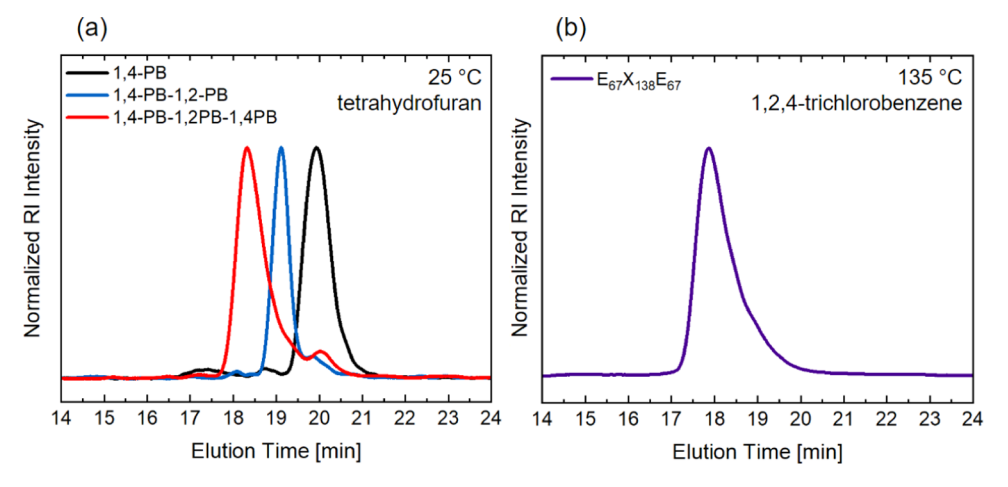


Figure 1. Normalized refractive index SEC data for the (a) PB precursors and (b) E₆₇X₁₃₈E₆₇ block copolymer.

Table 2. Characterization of the PE and PP Samples Used in This Work

sample code	$(kDa)^c$	D^c	$\binom{w_{ ext{PE}}}{(\%)}$	$w_{\mathrm{pp}} \ (\%)$	$T_{\mathrm{m,PE}} (^{\circ}\mathrm{C})$	$T_{m,PP}$ (°C)
PE ^a	32	3.1	100	0	129 ^f	117 ^f
PP^a	110	4.2	0	100	161 ^f	118 ^f
rPE^{b}	22	5.5	85	15 ^d	133 ^g	165 ^g
rPP^{b}	49	3.7	10	90 ^e	129 ^g	163 ^g

"Obtained from the Dow Chemical Company. ^bPost-consumer recycled resin provided by KW Plastics. ^cMeasured by SEC with TCB as the mobile phase at 150 °C and using light scattering detection with dn/dc = -0.110 and -0.103 mL/g. ^dFrom manufacturer data sheet and using DSC and AFM image analysis. ^cEstimated using DSC and AFM image droplet size analysis. ^fFrom ref 25. ^gDetermined by DSC while heating at 10 °C/min.

Table 2, and the two methods were found to be in good agreement within the expected uncertainty of about $\pm 5\%$ (see Table S5).

Small amplitude oscillatory shear experiments were performed in the linear viscoelastic regime on both virgin and recycled PE and PP. For the virgin PE and PP, complex viscosity as a function of frequency was analyzed using the Cross model and assuming the Cox–Merz rule. This yielded zero-shear viscosities of 2.83 and 30.7 kPa·s for PE and PP,

respectively (Figure S7 and Table S6). The frequency-dependent complex viscosity of the rPE and rPP samples could not be fit to the cross model, obviating the extraction of zero shear viscosities (Figure S8). We attribute this behavior to the phase-separated polyolefin impurities and possibly other unknown additives reflected in the black (rPE) and gray (rPP) sample colors.

3.3. Modification of rPE and rPP Using $E_{67}X_{138}E_{67}$. 1 wt % $E_{67}X_{138}E_{67}$ was added to rPE and rPP in order to compatibilize the minority impurity phases with the majority matrix phases. This section summarizes AFM phase images that reveal the specimen morphologies and tensile test results that establish the efficacy of compatibilization.

3.3.1. Morphology. Identically prepared samples of rPE and rPP with and without $E_{67}X_{138}E_{67}$ were cryo-microtomed and imaged using AFM, and the resulting phase images are shown in Figure 3. In these images, the more dissipative PE is darker than iPP, providing contrast. All images clearly show the presence of two phases in agreement with the DSC data presented in Figure 2. No statistically significant differences in average particle diameter were observed for neat rPE ($D_{\rm av}=0.90\pm0.30~\mu{\rm m}$) or rPP ($D_{\rm av}=0.61\pm0.30~\mu{\rm m}$) versus the $E_{67}X_{138}E_{67}$ -modified counterparts, ($D_{\rm av}=0.86\pm0.30~\mu{\rm m}$ and $D_{\rm av}=0.64\pm0.30~\mu{\rm m}$ for compatibilized rPE and rPP, respectively) (see Table S9). Here, we note that the particle

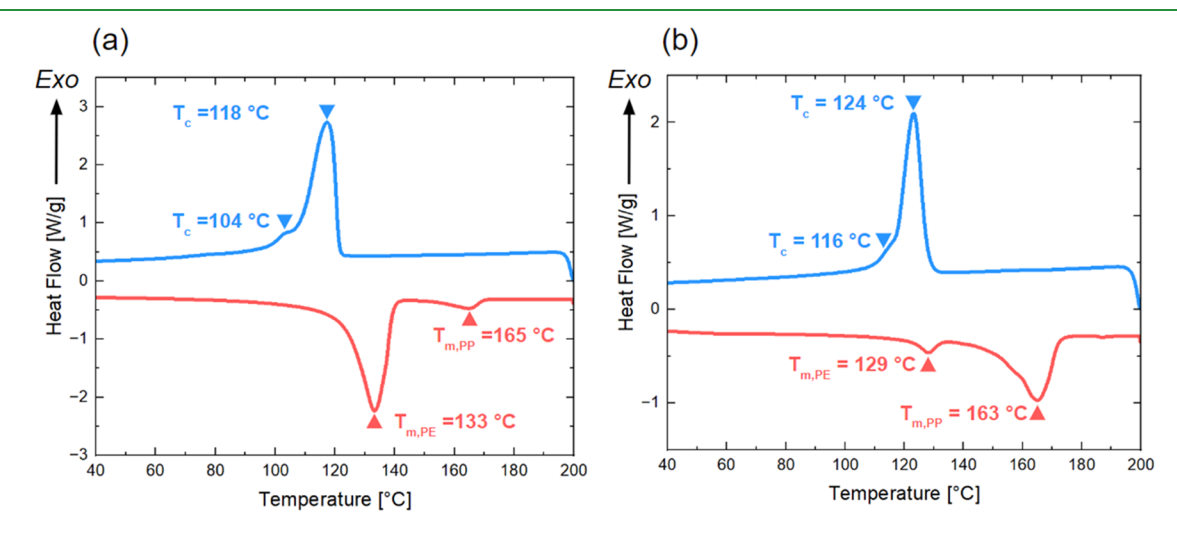


Figure 2. DSC heating (red) and cooling (blue) traces for (a) rPE and (b) rPP.

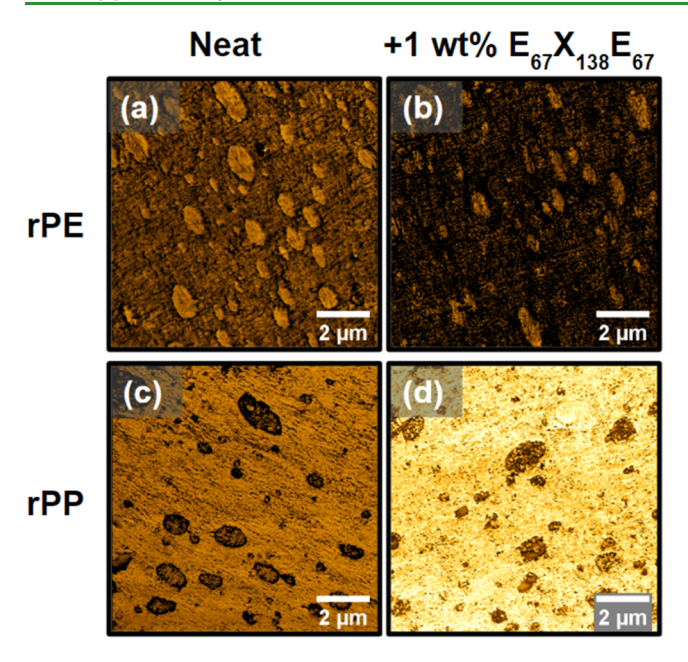


Figure 3. Representative AFM phase images of neat and compatible rPE (top row) and rPP (bottom row), where all samples underwent very fast cooling (~380 °C/min).

diameters were not significantly influenced by the choice of cooling profile, as shown in Figure S16.

3.3.2. Mechanical Properties of $E_{67}X_{138}E_{67}$ -Modified rPE and rPP. The efficacy of $E_{67}X_{138}E_{67}$ as a compatibilizer for producing useful mixed plastic waste was elucidated through the tensile testing of rPE and rPP, as shown in Figure 4. We begin by describing tensile properties at the fast cooling rate (38 °C/min), similar to previous research. The insets in Figure 4 show that the phase-separated structure of neat rPE with ~15% PP content and neat rPP with ~10% PE content results in brittle mechanical properties with strains at break of ε_b ~ 15% at the fast cooling rate, attributable to interfacial failure. At the fast cooling rate, $E_{67}X_{138}E_{67}$ imparts modest ductility to the rPE sample, increasing the average strain at break from 20 to 90% (inset in Figure 4a). Within experimental error, $E_{67}X_{138}E_{67}$ does not improve the toughness of the fast-cooled rPP (inset in Figure 4b). Sample failure in

rPP is accompanied by craze-like deformation with virtually no necking (see embedded photos in Figure S13b,d). Conversely, the fast-cooled rPE, shown in Figure 4a exhibited clear necking behavior (see the embedded photos in Figure S13a,c).

In contrast, preparing the samples using very fast cooling (380 °C/min), a cooling rate representative of industrial practice, resulted in much greater strains at break (Figures 4 and S14, and Table 3). The unmodified rPE and rPP were noticeably tougher than with the fast cooling rate, accompanied by a small decrease in modulus and yield stress (Table 3), likely due to a reduction in crystallinity at higher cooling rates. However, with the addition of 1 wt % $E_{67}X_{138}E_{67}$, both rPE and rPP demonstrated extraordinary toughness, increasing the strain at break to 700 and 600%, respectively. While the unmodified rPE and rPP also reached higher strains-at-break on average from very fast cooling compared to fast cooling, the standard deviation of the strain at break values was larger (> $\pm 100\%$) across samples, and they did not exhibit strain-hardening compared to compatibilized samples.

SEM images shown in Figure S15 were used to characterize fractured very fast-cooled tensile PCR specimens with and without $\rm E_{67}X_{138}E_{67}$. Between the uncompatibilized and compatibilized rPE, there is not a noticeable difference in debonding behavior at the particle—matrix interface. However, in the case of rPP, the compatibilized samples show a lower extent of particle debonding behavior compared to neat rPP and the phase-separated particles deforming with the matrix.

3.4. $\tilde{E}_{67}X_{138}E_{67}$ in a PE/iPP Blend of Virgin Resins. Adding $E_{67}X_{138}E_{67}$ to rPE and rPP resulted in a cooling rate-dependent material toughness. To evaluate the generality of this result and establish that this was not due to the presence of undefined additives and fillers in the PCR materials, the compatibilization efficacy of $E_{67}X_{138}E_{67}$ was explored with virgin PE/PP blends using the fast cooling procedure. This additionally enables direct comparisons with previously reported results using $E_{65}X_{88}E_{65}^{2.5}$.

Blends of virgin PE and PP (70:30 PE: PP) were prepared with 1 wt % $E_{67}X_{138}E_{67}$, and the corresponding uniaxial tensile stress—strain data are shown in Figures 5a and S11 and summarized in Table S7. In both PE- and PP-rich blends, $E_{67}X_{138}E_{67}$ imparts a clear improvement in the tensile strain at break compared to the unmodified blends shown in the inset

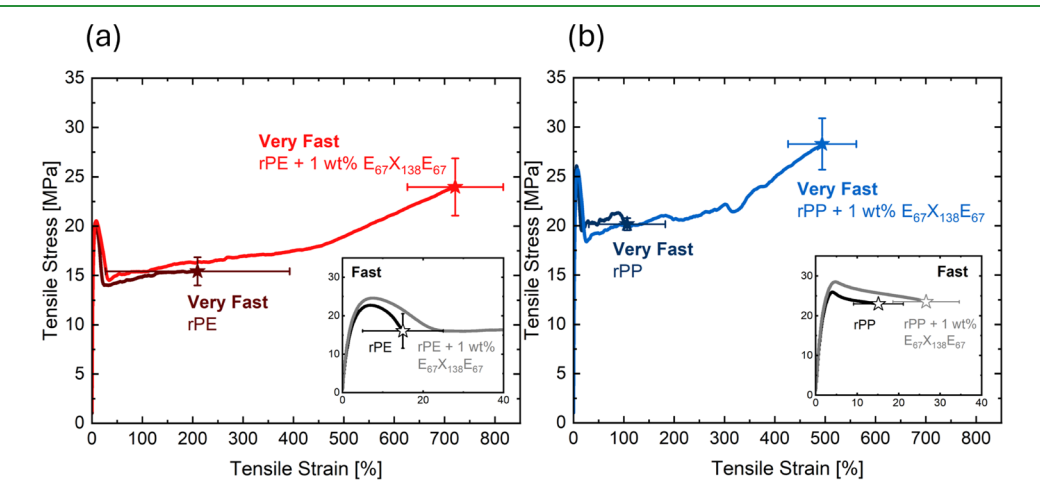


Figure 4. Representative stress—strain data demonstrating tensile toughness with and without 1 wt % $E_{67}X_{138}E_{67}$ in (a) rPE and (b) rPP when subjected to fast (38 °C/min) and very fast (380 °C/min) cooling of the melt-molded specimens. All scale bars represent one standard deviation from the mean based on at least 5 replicates.

Table 3. Mechanical Property Values^a for rPE and rPP Samples with and without $E_{67}X_{138}E_{67}$

	sample	E (GPa)	$\sigma_{ m y}~({ m MPa})$	$arepsilon_{ m b}$ (%)	$\sigma_{\rm b}~({ m MPa})$
fast-cooled	rPE	1.24 ± 0.04	23.0 ± 0.4	18 ± 10	16.7 ± 4.5
	rPE + 1 wt % EXE	1.33 ± 0.03	24.6 ± 0.2	99 ± 24	16.8 ± 0.3
	rPP	1.45 ± 0.04	25.6 ± 0.6	13 ± 6	22.9 ± 0.5
	rPP + 1 wt % EXE	1.46 ± 0.05	27.3 ± 0.7	28 ± 8	22.5 ± 0.8
very fast-cooled	rPE	1.14 ± 0.03	19.9 ± 0.4	205 ± 183	14.7 ± 1.4
	rPE + 1 wt % EXE	1.09 ± 0.04	21.1 ± 1.5	663 ± 95	21.9 ± 2.9
	rPP	1.25 ± 0.03	25.0 ± 0.5	101 ± 76	19.7 ± 0.6
	rPP + 1 wt % EXE	1.12 ± 0.03	24.6 ± 0.9	480 ± 68	26.5 ± 2.6

^a± Values represent standard deviations of at least 7 replicates, as shown in Figures S13 and S14.

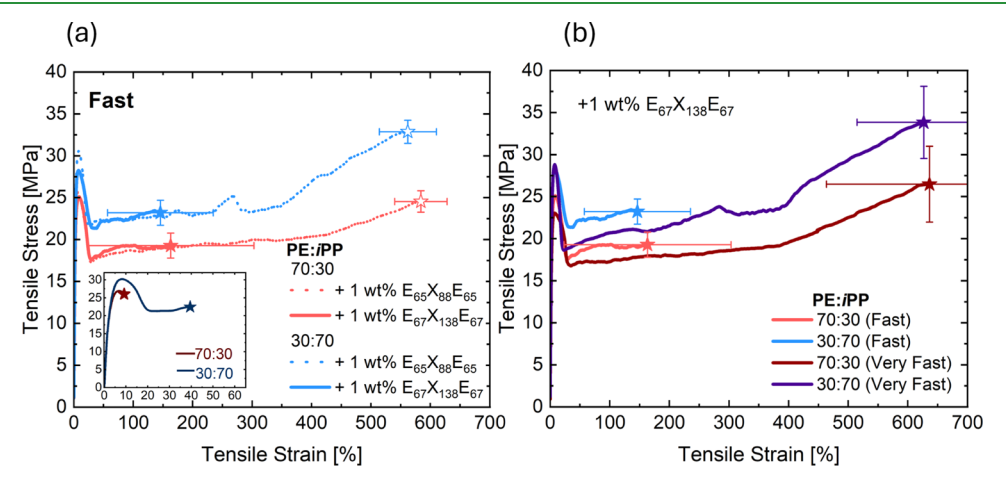


Figure 5. Representative stress—strain data comparing (a) the performance (using only the fast cooling profile) of $E_{65}X_{88}E_{65}$ and $E_{67}X_{138}E_{67}$ compared to neat 70:30 blends using virgin PE and PP and (b) the performance of virgin PE and PP blends that have been either fast or very fast-cooled (see Figure S10). The inset in (a) shows uncompatibilized blends. The $E_{65}X_{88}E_{65}$ data in (a) is from ref 25. All error bars represent one standard deviation from the mean based on at least 5 replicates.

of Figure 4a, increasing from 10 to 150% and 45 to 145%, respectively. However, the strain-at-break data exhibit large standard deviations, especially when compared to the $E_{65}X_{88}E_{65}$ -compatibilized blends, also shown in Figure 5a. These gains in toughness were accompanied by up to a 10% reduction in both the elastic modulus and yield stress (Table 3). Additionally, the blends modified with $E_{67}X_{138}E_{67}$ also consistently failed before strain hardening regardless of the majority component.

Increasing the cooling rate of the 1% $E_{67}X_{138}E_{67}$ -modified PE/PP melt-molded blends to 380 °C/min (very fast cooling) had a dramatic effect on the resulting mechanical properties, as shown in Figure 5b, similar to what was found with the recycled plastics (Figure 4). Strain at break for the PE and PP continuous mixtures increased to $\varepsilon_b > 600\%$, comparable to what was obtained with $E_{65}X_{88}E_{65}$ following fast cooling (38 °C/min). This comparison demonstrates that the requirement for very fast cooling with $E_{67}X_{138}E_{67}$ to produce tough blends is not a consequence of using PCR resins or due to cooling rate effects on bulk blend component properties but reflects different size X blocks and hence different copolymer compositions between the two triblocks since the E blocks have nearly identical molecular weights.

4. DISCUSSION

The dramatic toughness enhancement in rPE and rPP afforded by the addition of only 1 wt % EXE (Figure 4) triblock copolymer compatibilizer suggests these materials offer a promising avenue to recover value in mixed plastic waste streams. Importantly, the efficacy of these additives did not appear to be impacted negatively by the presence of fillers, pigments, dyes, and other residues from their previous uses even though they may be expected to present significant interfacial area and augment thermodynamic interactions compared to virgin materials; it is also important to appreciate that the additives present in recyclates will vary depending on their source.

The mechanical performance of the $E_{67}X_{138}E_{67}$ modified materials was cooling-rate-dependent in the PE/PP blends and both rPE and rPP. This indicates that the origins of the differences in mechanical behavior between $E_{67}X_{138}E_{67}$ and $E_{65}X_{88}E_{65}$, in both sets of materials, lie with the difference in triblock structure, specifically the longer X block in the former polymer. While we do not have a definitive cause for this surprising effect, several plausible explanations are advanced here

We first hypothesize that the larger X block, hence larger fraction of the PP-miscible portion of the triblock, may favor micelle formation, which would reduce the amount of interfacial coverage, thereby degrading compatibilization. Micelles are likely to be most stable in the PE phase, where center X blocks would form the cores and the tethered E blocks the corona. Creating micelles in PP would require a flower-like configuration with looping X blocks in the corona, a less favorable molecular configuration. Sequestering the triblock in micelles would decrease the transport to the PE/PP interfaces during melt mixing and annealing at elevated temperatures during specimen molding. While we did not

identify micelles in the AFM images, this is not too surprising given the low concentration of block copolymer (1 wt %). We performed a preliminary test of this hypothesis by increasing the concentration of $E_{67}X_{138}E_{67}$ to 1.7 wt % in the PE/PP blends and repeating the tensile experiments under the fast cooling (38 °C/min) condition. As shown in Figure 6, this

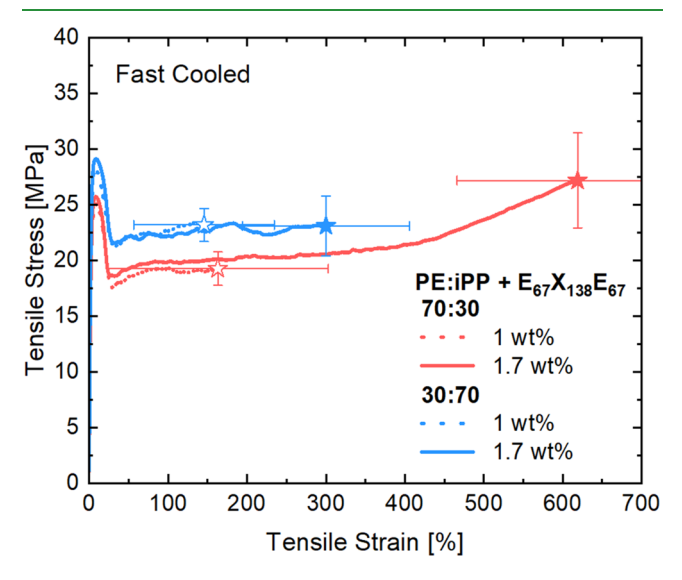


Figure 6. Representative stress—strain data of fast-cooled virgin 70:30 blends comparing the performance of $E_{67}X_{138}E_{67}$ at 1 and 1.7 wt %. All error bars represent one standard deviation from the mean based on at least 5 replicates.

produced a dramatic increase in the strain at break in the 70:30 PE/PP blend, $\varepsilon_{\rm b}=600\%$, comparable to what was obtained with E₆₅X₈₈E₆₅ at 1 wt % loading (Figure 5). The 30:70 PE/PP blend also improved slightly with the higher triblock loading, $\varepsilon_{\rm b}=300\%$, although this does not match the result with E₆₅X₈₈E₆₅ at 1 wt % (Figure 5). If the micelle hypothesis has merit, increasing the triblock concentration should drive more block copolymer to the PE/PP interfaces, thereby providing greater coverage, which would translate to greater interfacial strength. Clearly, if micelles do form, then diffusion to the PE/PP interfaces would be greatly hampered. Additional work needs to be done to establish how triblock composition and overall molecular weight control micelle formation and transport to the phase-separated domain boundaries.

An alternative explanation involves the mixing process in the lab-scale twin screw extruder. The two triblock copolymers have different compositions, $f_{\rm X}=0.40$ and $f_{\rm X}=0.51$ for ${\rm E}_{65}{\rm X}_{88}{\rm E}_{65}$ and ${\rm E}_{67}{\rm X}_{138}{\rm E}_{67}$, respectively, where $f_{\rm X}$ is the volume fraction of the X block in the melt state; we assume E and X have equal melt densities. This difference in composition may lead to different melt morphologies, which could significantly influence the breakup and dispersion of the triblock during blending, e.g., a cylindrical morphology would shear differently than lamellae. Unfortunately, we were not able to characterize the melt morphologies by small-angle X-ray scattering due to contrast matching between the E and X blocks in the melt

Another possibility is that the larger X block in $E_{67}X_{138}E_{67}$ results in less favorable molecular configurations at the PE/PP interfaces. We have no basis for arguing what the ideal EXE composition would be to best accommodate the interfacial curvature in competition with micelle formation. However, in

the limits of large or small $f_{\rm X}$, localization at relatively flat domain boundaries would not be favored. Apparently $f_{\rm X}=0.40$ works better than $f_{\rm X}=0.51$. This hypothesis should be testable using molecular simulations, and we expect that interfacial molecular configurations will be influenced by conformational asymmetry differences of E and X, and the thermodynamically favored side of the interface occupied by the loop and end blocks, relative to the direction of interfacial curvature.

Finally, the proposed "threading the needle" mechanism of interfacial strengthening may be influenced by block copolymer composition. On the PP side of the domain boundary, we have proposed that the constrained molecular configurations of the X blocks (attached on each end to E blocks) in the melt state lead to topological trapping of chains in the amorphous part of PP when crystallized upon cooling. Perhaps the larger X block in E₆₇X₁₃₈E₆₇ is less effective at capturing PP chains during crystallization due to a larger loop size. The cooling rate dependence of $\varepsilon_{\rm b}$ might be explained by this mechanism. At the slower cooling rate, PP chains will have more time to localize adjacent to chain folded crystals, possibly facilitated by the greater volume occupied by the X blocks, which may allow PP chains to more easily "unthread" the eye of the needle. While this argument seems consistent with the observed trends, it would be surprising if the modest change in X block molecular weight caused such behavior. On the other side of the interface, the triblock copolymers are speculated to be anchored in place by E block cocrystallization with PE homopolymer. We do not believe that the E blocks play a role in the observed mechanical property differences given that both triblocks share common E block molecular weights.

Regardless of the actual reason for the documented differences between $E_{67}X_{138}E_{67}$ and $E_{65}X_{88}E_{65}$, both compounds are effective compatibilizers for PE/PP blends, and EXE in general provides outstanding value in recovering ductility in recycled PE and PP plastics.

5. CONCLUSIONS

Reintroduction of mixed PE and PP post-consumer waste streams into the economy has traditionally been riddled with practical and economic complications. By leveraging anionic polymerization of butadiene and subsequent catalytic hydrogenation, industrially practiced synthesis methods, EXE block copolymers present an attractive approach to recovering useful mechanical properties in recycled PE and PP. This study showcases EXE's potential as a compatibilizer in postconsumer recycled rPE and rPP and exposes limitations set by the X block molecular weight at constant E block molecular weight. Addition of 1 wt % of E₆₇X₁₃₈E₆₇ to commercially available brittle rPE and rPP, with approximate purity of 85-90%, leads to highly ductile plastics with strains at break $\varepsilon_{\rm b}$ > 500%. However, this degree of compatibilization required very fast cooling of melt-molded specimens (380 °C/min), a cooling rate that is consistent with industrial practice. Comparison of the efficacy of $E_{67}X_{138}E_{67}$ and $E_{65}X_{88}E_{65}$ in toughening blends of virgin PE and PP revealed a significant dependence on the X block molecular weight. Several hypotheses are advanced to explain this behavior, most notably the possibility of micelle formation, which would deplete the 2phase interfaces of essential triblock copolymer. We conclude that the EXE family of block copolymer compatibilizers requires additional research to optimize the molecular structure and understand its broader range of compatibilization performance, e.g., in creep, fatigue, and impact tests, and as a

function of aging. This work offers exciting opportunities to build a more sustainable plastics economy.

ASSOCIATED CONTENT

Supporting Information

The Supporting Information is available free of charge at https://pubs.acs.org/doi/10.1021/acsapm.4c02270.

Synthesis and characterization details of compatibilizers; thermal analysis and composition characterization of PE/PP homopolymers/blends and rPE and rPP recyclates, with and without added compatibilizers; experimental protocols and characterization of cooling rates during sample preparation; tensile test data for PE/PP homopolymers/blends and rPE and rPP recyclates, with and without added compatibilizers; summaries of mechanical properties; and images and analysis of dispersed phases after melt processing and tensile testing (PDF)

AUTHOR INFORMATION

Corresponding Authors

Christopher J. Ellison – Department of Chemical Engineering and Materials Science, University of Minnesota, Minneapolis, Minnesota 55455, United States; orcid.org/0000-0002-0393-2941; Email: cellison@umn.edu

Frank S. Bates – Department of Chemical Engineering and Materials Science, University of Minnesota, Minneapolis, Minnesota 55455, United States; oorcid.org/0000-0003-3977-1278; Email: bates001@umn.edu

Authors

Gabriela Díaz Gorbea — Department of Chemical Engineering and Materials Science, University of Minnesota, Minneapolis, Minnesota 55455, United States; orcid.org/0000-0003-3600-4567

Liyang Shen – Department of Chemical Engineering and Materials Science, University of Minnesota, Minneapolis, Minnesota 55455, United States; orcid.org/0000-0001-9928-2877

Kendra Flanigan – Department of Chemical Engineering and Materials Science, University of Minnesota, Minneapolis, Minnesota 55455, United States

Complete contact information is available at: https://pubs.acs.org/10.1021/acsapm.4c02270

Notes

The authors declare no competing financial interest.

■ ACKNOWLEDGMENTS

The authors thank the National Science Foundation grant DMR-2304179 and the Center for Sustainable Polymers, an NSF-supported Center for Chemical Innovation (CHE-1901635), for financial support. Parts of the work were carried out in the Characterization Facility, University of Minnesota, which receives partial support from the NSF through the MRSEC (Award Number DMR-2011401) and the NNCI (Award Number ECCS-2025124) programs.

■ REFERENCES

(1) Franklin Associates, A. D. of E. R. G.. Life Cycle Impacts of Plastic Packaging Compared to Substritutes in the United States and Canada: Theoretical Substitution Analysis, The Plastics Division of the American

- Chemistry Council (ACC), 2018. 172. https://www.americanchemistry.com/content/download/7885/file/Life-Cycle-Impacts-of-Plastic-Packaging-Compared-to-Substitutes-in-the-United-States-and-Canada.pdf.
- (2) Billiet, S.; Trenor, S. R. 100th Anniversary of Macromolecular Science Viewpoint: Needs for Plastics Packaging Circularity. *ACS Macro Lett.* **2020**, *9* (9), 1376–1390.
- (3) Bremer, C. Plastic Pollution Is Growing Relentlessly as Waste Management and Recycling Fall Short; Says OECD. 2022.
- (4) Geyer, R.; Jambeck, J. R.; Law, K. L. Production, Use, and Fate of All Plastics Ever Made. Sci. Adv. 2017, 3 (7), No. e1700782.
- (5) Vogt, B. D.; Stokes, K. K.; Kumar, S. K. Why Is Recycling of Postconsumer Plastics so Challenging? *ACS Appl. Polym. Mater.* **2021**, 3 (9), 4325–4346.
- (6) United States Environmental Protection Agency. Advancing Sustainable Materials Management: Facts and Figures Report, Advancing Sustainable Materials Management: 2018 Tables and Figures Assessing Trends in Materials Generation and Management in the United States, United States Environmental Protection Agency2020. https://www.epa.gov/facts-and-figures-about-materials-waste-and-recycling/advancing-sustainable-materials-management.
- (7) Working group "Design for Recycling" under the Danish Plastics Federation's Forum for Circular Plastic Packaging: Arla Foods, COOP, the Danish Technological Institute, the City of Copenhagen, UPM Raflatac, Færch Plast, Plus Pack, BEWI, RPC Superfos, Trioplast, Kellpo, Ecolabelling Denmark, the Danish Society for Nature Conservation, Circle Development and Stena Recycling, Reuse and Recycling of Plastic Packaging for Private Use, Forum for Circular Plastic Packaging under the Danish Plastics Federation, 2015. https://plast.dk/wp-content/uploads/2018/09/Design-Manual-Reuse-and-recycling-of-plastic-packaging-for-private-use.pdf.
- (8) Lase, I. S.; Tonini, D.; Caro, D.; Albizzati, P. F.; Cristóbal, J.; Roosen, M.; Kusenberg, M.; Ragaert, K.; Van Geem, K. M.; Dewulf, J.; De Meester, S. How Much Can Chemical Recycling Contribute to Plastic Waste Recycling in Europe? An Assessment Using Material Flow Analysis Modeling. *Resour., Conserv. Recycl.* 2023, 192, No. 106916.
- (9) Uekert, T.; Singh, A.; DesVeaux, J. S.; Ghosh, T.; Bhatt, A.; Yadav, G.; Afzal, S.; Walzberg, J.; Knauer, K. M.; Nicholson, S. R.; Beckham, G. T.; Carpenter, A. C. Technical, Economic, and Environmental Comparison of Closed-Loop Recycling Technologies for Common Plastics. ACS Sustainable Chem. Eng. 2023, 11 (3), 965–978
- (10) Serranti, S.; Bonifazi, G. Techniques for Separation of Plastic Wastes. In *Use of Recycled Plastics in Eco-efficient Concrete*; Elsevier, 2019; pp 9–37.
- (11) Zervoudakis, A. J.; Sample, C. S.; Peng, X.; Lake, D.; Hillmyer, M. A.; Ellison, C. J. Dihydroxy Polyethylene Additives for Compatibilization and Mechanical Recycling of Polyethylene Terephthalate/Polyethylene Mixed Plastic Waste. *ACS Macro Lett.* **2022**, *11* (12), 1396–1402.
- (12) Self, J. L.; Zervoudakis, A. J.; Peng, X.; Lenart, W. R.; Macosko, C. W.; Ellison, C. J. Linear, Graft, and Beyond: Multiblock Copolymers as Next-Generation Compatibilizers. *JACS Au* **2022**, 2 (2), 310–321.
- (13) Peng, X.; Shin, Y.; Zervoudakis, A. J.; Nomura, K.; Lindenmeyer, K. M.; Miller, K. M.; Ellison, C. J. Poly(Ethylene Terephthalate)-polyethylene Block Copolymer Architecture Effects on Interfacial Adhesion and Blend Compatibilization. *J. Polym. Sci.* **2023**, *62*, 753–765.
- (14) Nomura, K.; Peng, X.; Kim, H.; Jin, K.; Kim, H. J.; Bratton, A. F.; Bond, C. R.; Broman, A. E.; Miller, K. M.; Ellison, C. J. Multiblock Copolymers for Recycling Polyethylene—Poly(Ethylene Terephthalate) Mixed Waste. ACS Appl. Mater. Interfaces 2020, 12 (8), 9726—9735.
- (15) Adedeji, A.; Lyu, S.; Macosko, C. W. Block Copolymers in Homopolymer Blends: Interface vs Micelles. *Macromolecules* **2001**, 34 (25), 8663–8668.

- (16) Lyu, S.; Jones, T. D.; Bates, F. S.; Macosko, C. W. Role of Block Copolymers on Suppression of Droplet Coalescence. *Macromolecules* **2002**, 35 (20), 7845–7855.
- (17) Macosko, C. W.; Guégan, P.; Khandpur, A. K.; Nakayama, A.; Marechal, P.; Inoue, T. Compatibilizers for Melt Blending: Premade Block Copolymers. *Macromolecules* **1996**, *29* (17), 5590–5598.
- (18) Khalili, R.; Jafari, S. H.; Saeb, M. R.; Khonakdar, H. A.; Wagenknecht, U.; Heinrich, G. Toward In Situ Compatibilization of Polyolefin Ternary Blends through Morphological Manipulations. *Macromol. Mater. Eng.* **2014**, 299 (10), 1197–1212.
- (19) Xanthos, M.; Dagli, S. S. Compatibilization of Polymer Blends by Reactive Processing. *Polym. Eng. Sci.* **1991**, *31* (13), 929–935.
- (20) Arriola, D. J.; Carnahan, E. M.; Hustad, P. D.; Kuhlman, R. L.; Wenzel, T. T. Catalytic Production of Olefin Block Copolymers via Chain Shuttling Polymerization. *Science* **2006**, *312* (5774), 714–719.
- (21) Xu, J.; Eagan, J. M.; Kim, S.-S.; Pan, S.; Lee, B.; Klimovica, K.; Jin, K.; Lin, T.-W.; Howard, M. J.; Ellison, C. J.; LaPointe, A. M.; Coates, G. W.; Bates, F. S. Compatibilization of Isotactic Polypropylene (*i* PP) and High-Density Polyethylene (HDPE) with *i* PP–PE Multiblock Copolymers. *Macromolecules* **2018**, *51* (21), 8585–8596.
- (22) Eagan, J. M.; Xu, J.; Di Girolamo, R.; Thurber, C. M.; Macosko, C. W.; LaPointe, A. M.; Bates, F. S.; Coates, G. W. Combining Polyethylene and Polypropylene: Enhanced Performance with PE/ *i* PP Multiblock Polymers. *Science* **2017**, 355 (6327), 814–816.
- (23) Klimovica, K.; Pan, S.; Lin, T.-W.; Peng, X.; Ellison, C. J.; LaPointe, A. M.; Bates, F. S.; Coates, G. W. Compatibilization of *i* PP/HDPE Blends with PE- *g i* PP Graft Copolymers. *ACS Macro Lett.* **2020**, *9* (8), 1161–1166.
- (24) Wolff, P.; Dickert, A.; Kretschmer, W. P.; Kempe, R. I PP/PE Multiblock Copolymers for Plastic Blend Recycling Synthesized by Coordinative Chain Transfer Polymerization. *Macromolecules* **2022**, 55 (15), 6435–6442.
- (25) Shen, L.; Gorbea, G. D.; Danielson, E.; Cui, S.; Ellison, C. J.; Bates, F. S. Threading-the-Needle: Compatibilization of HDPE/ *i* PP Blends with Butadiene-Derived Polyolefin Block Copolymers. *Proc. Natl. Acad. Sci. U.S.A.* **2023**, *120* (34), No. e2301352120.
- (26) Frederickson, G. H.; Liu, A. J.; Bates, F. S. Entropic corrections to the Flory-Huggins theory of polymer blends: Architectural and conformational effects effects. *Macromolecules* **1994**, 27, 2503–2511.
- (27) Weimann, P. A.; Jones, T. D.; Hillmyer, M. A.; Bates, F. S.; Londono, J. D.; Melnichenko, Y.; Wignall, G. D.; Almdal, K. Phase Behavior of Isotactic Polypropylene–Poly(Ethylene/Ethylethylene) Random Copolymer Blends. *Macromolecules* **1997**, *30* (12), 3650–3657
- (28) Osborn, J. A.; Jardine, F. H.; Young, J. F.; Wilkinson, G. The Preparation and Properties of Tris(Triphenylphosphine)-Halogenorhodium(I) and Some Reactions Thereof Including Catalytic Homogeneous Hydrogenation of Olefins and Acetylenes and Their Derivatives. J. Chem. Soc. A 1966, 1711–1732.
- (29) Mohammadi, N. A.; Rempel, G. L. Homogeneous Catalytic Hydrogenation of Polybutadiene. *J. Mol. Catal.* **1989**, *50* (3), 259–275
- (30) Sun, T.; Brant, P.; Chance, R. R.; Graessley, W. W. Effect of Short Chain Branching on the Coil Dimensions of Polyolefins in Dilute Solution. *Macromolecules* **2001**, *34* (19), 6812–6820.
- (31) Lee, D.; Miller, M. D.; Meunier, D. M.; Lyons, J. W.; Bonner, J. M.; Pell, R. J.; Shan, C. L. P.; Huang, T. Development of High Temperature Comprehensive Two-Dimensional Liquid Chromatography Hyphenated with Infrared and Light Scattering Detectors for Characterization of Chemical Composition and Molecular Weight Heterogeneities in Polyolefin Copolymers. *J. Chromatogr. A* **2011**, 1218 (40), 7173–7179.
- (32) Jackson, C.; Chen, Y.-J.; Mays, J. W. Size Exclusion Chromatography with Multiple Detectors: Solution Properties of Linear Chains of Varying Flexibility in Tetrahydrofuran. *J. Appl. Polym. Sci.* **1996**, *61* (5), 865–874.
- (33) Kraus, G.; Stacy, C. J. Molecular Weight and Long-chain Branching Distributions of Some Polybutadienes and Styrene-

- Butadiene Rubbers. Determination by GPC and Dilute Solution Viscometry. J. Polym. Sci., Part A-2 1972, 10 (4), 657–672.
- (34) Galante, M. J.; Mandelkern, L.; Alamo, R. G. The Crystallization of Blends of Different Types of Polyethylene: The Role of Crystallization Conditions. *Polymer* **1998**, 39 (21), 5105–5119.
- (35) Quinn, F. A.; Mandelkern, L. Thermodynamics of Crystallization in High Polymers: Poly-(Ethylene) ¹. *J. Am. Chem. Soc.* **1958**, 80 (13), 3178–3182.
- (36) Lanyi, F. J.; Wenzke, N.; Kaschta, J.; Schubert, D. W. On the Determination of the Enthalpy of Fusion of α -Crystalline Isotactic Polypropylene Using Differential Scanning Calorimetry, X-Ray Diffraction, and Fourier-Transform Infrared Spectroscopy: An Old Story Revisited. *Adv. Eng. Mater.* **2020**, 22 (9), No. 1900796.
- (37) Chaffin, K. A.; Bates, F. S.; Brant, P.; Brown, G. M. Semicrystalline Blends of Polyethylene and Isotactic Polypropylene: Improving Mechanical Performance by Enhancing the Interfacial Structure. J. Polym. Sci., Part B: Polym. Phys. 2000, 38 (1), 108–121.